Ultrahigh-throughput magnetic sorting of large blood volumes for epitope-agnostic isolation of circulating tumor cells

Avanish Mishra[a,b,c,d,1], Taronish D. Dubash[c,d,1], Jon F. Edd[a,b,c], Michelle K. Jewett[a,b,c], Suhaas G. Garre[a,b,c], Nezihi Murat Karabacak[a,b,e], Daniel C. Rabe[a,b,c,d], Baris R. Mutlu[a,b,d], John R. Walsh[a,b,c], Ravi Kapur[f], Shannon L. Stott[a,b,c,d], Shyamala Maheswaran[c,d], Daniel A. Haber[c,d,g,2], and Mehmet Toner[a,b,d,e,2]

[a]BioMEMS Resource Center, Charlestown, MA 02129; [b]Center for Engineering in Medicine and Surgery, Massachusetts General Hospital, Boston, MA 02114; [c]Cancer Center, Massachusetts General Hospital, Boston, MA 02114; [d]Harvard Medical School, Boston, MA 02115; [e]Shriners Hospitals for Children, Boston, MA 02114; [f]MicroMedicine, Inc., Waltham, MA 02451; and [g]Howard Hughes Medical Institute, Bethesda, MD 20815

Contributed by Daniel A. Haber, May 13, 2020 (sent for review April 10, 2020; reviewed by James J. Collins and John A. Rogers)

Circulating tumor cell (CTC)-based liquid biopsies provide unique opportunities for cancer diagnostics, treatment selection, and response monitoring, but even with advanced microfluidic technologies for rare cell detection the very low number of CTCs in standard 10-mL peripheral blood samples limits their clinical utility. Clinical leukapheresis can concentrate mononuclear cells from almost the entire blood volume, but such large numbers and concentrations of cells are incompatible with current rare cell enrichment technologies. Here, we describe an ultrahigh-throughput microfluidic chip, ^{LP}CTC-iChip, that rapidly sorts through an entire leukapheresis product of over 6 billion nucleated cells, increasing CTC isolation capacity by two orders of magnitude (86% recovery with 10^5 enrichment). Using soft iron-filled channels to act as magnetic microlenses, we intensify the field gradient within sorting channels. Increasing magnetic fields applied to inertially focused streams of cells effectively deplete massive numbers of magnetically labeled leukocytes within microfluidic channels. The negative depletion of antibody-tagged leukocytes enables isolation of potentially viable CTCs without bias for expression of specific tumor epitopes, making this platform applicable to all solid tumors. Thus, the initial enrichment by routine leukapheresis of mononuclear cells from very large blood volumes, followed by rapid flow, high-gradient magnetic sorting of untagged CTCs, provides a technology for noninvasive isolation of cancer cells in sufficient numbers for multiple clinical and experimental applications.

circulating tumor cells | microfluidics | magnetic sorting | leukapheresis | liquid biopsy

Approximately 90% of cancer-related deaths are attributable to metastatic disease, most commonly resulting from the blood-borne dissemination of circulating tumor cells (CTCs) (1, 2). CTCs are actively shed into the blood from primary and metastatic tumor deposits, both as single cancer cells or as clusters (3). Most CTCs have a limited half-life and do not survive the high physical and oxidative stress within the blood circulation, but a small fraction of cells remain viable and initiate metastatic lesions in distal organs (4). Molecular studies of these metastatic precursors, which can be cultured ex vivo, provide insight into the biology of cancer cell invasion and dissemination (5). In addition to this metastasis-competent subset of cancer cells in the blood, all intact CTCs provide a rich source of molecular markers with which to monitor cancer progression and evolution under therapeutic pressure (6–9). Thus, blood sampling for CTCs during the course of treatment may identify the acquisition of simple somatic mutations or complex DNA alterations and changes in RNA or protein composition that provide pharmacokinetic measurements of on-target drug effects (10, 11). While CTC-based assays have the potential to uncover a wide range of cancer-related biomarkers for "real-time" clinical applications, their deployment has been hampered by the very rare number of cancer cells present within a standard blood tube, limiting analytic reliability.

Among the most promising CTC enrichment technologies are microfluidic devices, whose efficient and low-stress processing maximizes the chance of viable CTC recovery (12). Various microfluidic platforms have been developed, selecting for CTCs based on their physical attributes, size (13–15) and deformability (16, 17), and immunochemical cell surface markers (18). Instead of positive selection of CTCs based on such predefined properties, which are highly heterogeneous in cancer cells, we recently developed a "negative depletion" microfluidic chip (CTC-iChip) in which the magnetic sorting is sufficiently efficient to allow removal of tagged hematopoietic cells (19, 20). This leukocyte depletion strategy enriches for untagged CTCs in a "tumor-independent" manner, applicable to all tumor types, as demonstrated for breast (5), prostate (21), liver (9), melanoma (7), and lung (22) cancers. Nonetheless, extending from proof-of-principle biological studies to

Significance

Isolation of sufficient numbers of circulating tumor cells (CTCs) in cancer patients could provide an alternative to invasive tumor biopsies, providing multianalyte cell-based biomarkers that are not available from current plasma circulating tumor DNA sequencing. Given the average prevalence at one CTC per billion blood cells, very large blood volumes must be screened to provide enough CTCs for reliable clinical applications. By creating an ultrahigh-throughput magnetic sorter, we demonstrate the efficient removal of leukocytes from near whole blood volume equivalents. Combined with leukapheresis to initially concentrate blood mononuclear cells, this ^{LP}CTC-iChip platform will enable noninvasive sampling of cancer cells in sufficient numbers for clinical applications, ranging from real-time pharmacokinetic monitoring of drug response to tissue-of-origin determination in early-stage cancer screening.

Author contributions: A.M., T.D.D., J.F.E., S.M., D.A.H., and M.T. designed research; A.M., T.D.D., and M.K.J. performed research; S.G.G., N.M.K., D.C.R., J.R.W., and R.K. contributed new reagents/analytic tools; A.M., T.D.D., J.F.E., N.M.K., D.C.R., B.R.M., S.L.S., S.M., D.A.H., and M.T. analyzed data; and A.M., T.D.D., J.F.E., S.M., D.A.H., and M.T. wrote the paper.

Reviewers: J.J.C., Massachusetts Institute of Technology; and J.A.R., Northwestern University.

Competing interest statement: Massachusetts General Hospital has filed patent applications for the circulating tumor cell isolation technology described in this publication.

[1]A.M. and T.D.D. contributed equally to this work.

[2]To whom correspondence may be addressed. Email: dhaber@mgh.harvard.edu or mtoner@hms.harvard.edu.

This article contains supporting information online at https://www.pnas.org/lookup/suppl/doi:10.1073/pnas.2006388117/-/DCSupplemental.

First published July 8, 2020.

robust clinical applications requires analysis of larger blood volumes than are possible using currently available technologies (as demonstrated by statistical analysis in *SI Appendix*, Fig. S1).

A standard blood tube for diagnostic analysis contains 10 mL of peripheral blood, from which 1 to 50 CTCs may be isolated, depending on tumor type and stage of disease (22). While collecting large numbers of blood tubes from patients with cancer is prohibitive, leukapheresis is a well-tolerated routine clinical procedure (23, 24), in which large volumes of blood (~5 L) are processed, with centrifugal enrichment of peripheral blood mononuclear cells into a leukopak of ~65 mL volume during an hour-long procedure. The remaining constituents of the blood, including plasma, red blood cells (RBCs), and most neutrophils, are returned to the patient. CTCs, by virtue of having a similar density as mononuclear cells (1,050 to 1,080 kg/m^3), are enriched in the leukapheresis product (23).

While leukapheresis allows for initial cell density-based sorting of entire blood volumes, current CTC isolation technologies can only process up to 200 million mononuclear cells, or about 3 to 5% of a leukopak, significantly limiting the ultimate benefit of processing leukapheresis products (23–28). Here we describe a microfluidic chip, termed "^{LP}CTC-iChip," (LP: leukapheresis product) that can process the entire leukapheresis volume of 65 mL and is capable of recovering thousands of untagged viable CTCs by depleting RBCs, platelets, and white blood cells (WBCs) in a tumor-agnostic manner. The ^{LP}CTC-iChip consists of inertial separation array devices for removal of RBCs and platelets followed by a high-gradient magnetic cell sorter for the depletion of WBCs. The development of this ultrahigh-throughput permeability-enhanced magnetic cell sorter enables depletion of 50- to 100-fold more WBCs than current magnetic depletion platforms and is critical to the processing of large blood volumes for CTC enrichment at an unprecedented scale.

Results

Workflow for Microfluidic Isolation of CTCs from Leukapheresis Products. A typical 65-mL leukapheresis product derived from differential centrifugation of ~5 L of whole blood consists of 3 to 6 billion WBCs, with 10 to 30 billion contaminating RBCs. We calculate that leukopaks from patients with cancer are likely to also have 100 to 20,000 CTCs, depending on the type and stage of malignancy. WBCs consist primarily of mononuclear cells, since neutrophils are depleted by centrifugal forces during apheresis, and their concentration within the leukopak ranges from 50 to 90 million cells per mL, >10-fold higher than the WBC concentration in whole blood. Depending on the apheresis settings, the concentration of contaminating platelets may also be 10-fold higher in a leukopak, compared with whole blood. Altogether, the very high number of WBCs and platelets, concentrated within a large volume of leukapheresis product, presents a major challenge, compared to standard 10-mL samples of peripheral blood that are currently used for microfluidic enrichment of CTCs.

Fig. 1*A* illustrates the workflow that we established for depletion of hematopoietic cells from leukapheresis products. To process these complex samples, we first labeled WBCs with a mixture of biotinylated antibodies targeting the pan-leukocyte cell surface antigens CD45, CD16, CD3, CD45RA, and CD66b. The selection of antibodies against CD45, CD66b, and CD16 was based on our previous CTC isolation studies (19, 20), while CD3 and CD45RA antibodies were added to further deplete WBCs, based on mass cytometric profiling of contaminating cells in the product (*SI Appendix*, Fig. S2). Using a microfluidic device termed nonequilibrium inertial separation array (29), we achieved the removal of RBCs and platelets based on their small physical size, compared with nucleated cells (*SI Appendix*, Fig. S3). We then tagged the antibody-bound WBCs with 1-μm streptavidin-coated superparamagnetic beads and used the high-throughput magnetic sorter chip to deplete WBCs and recover unlabeled CTCs. The whole CTC isolation process is completed within 3 h.

Depletion of Erythrocytes and Platelets. The inertial separation array chip is based on our previous work (29) and exploits size-dependent inertial wall lift forces, proportional to the sixth power of the cell diameter, for efficient isolation of nucleated cells into a clean buffer. This device is designed as an array of rectangular islands (200 μm long × 50 μm wide × 52 μm tall) where cells are placed in close proximity to the walls (*SI Appendix*, Fig. S3*A*). Since wall-induced lift force is highly dependent on cell size, WBCs and CTCs undergo a greater deflection away from the wall than RBCs and platelets (*SI Appendix*, Fig. S3*A*). At the end of the rectangular island, a portion of the flow in the near-wall region is siphoned (3.6% of each main channel flow) through each of numerous narrow vertical gaps between one island and the next, thus removing the smaller cells (RBCs and platelets). This siphoning is repeated over the whole array to ensure a high yield of nucleated cells in the clean buffer and the effective removal of RBCs and platelets (*SI Appendix*, Fig. S3 *A* and *B*).

In contrast to deterministic lateral displacement (30), where cells cross streamlines when nudged by a post, the inertial separation array described above amplifies small cell size differences by allowing inertial lift forces to push cells away from the channel walls. In addition to its intrinsically faster blood processing, clogging is eliminated due to subsecond residence times and cell-free zones near channel walls. For this purpose, we used 32 parallel devices contained in two microfluidic plastic disks, created by using injection molding of cyclic olefin copolymer (*SI Appendix*, Fig. S3*C*). The total leukapheresis sample flow rate was 73 mL/h, while buffer was injected at 348 mL/h, enabling debulking of a whole 65-mL leukapheresis product within an hour. We note that bulk methods, such as density-gradient centrifugation and RBC lysis, are also widely used for removing RBCs from leukopaks. However, given their batch processing and lower specificity, these methods suffer from 27% and 11% loss of CTCs, respectively, compared with inertial separation array devices (31). After debulking, we labeled WBCs with magnetic beads and used the magnetic sorter for depleting WBCs.

Design of an Ultrahigh-Throughput Magnetic Sorter for Depletion of WBCs. Isolating hundreds to thousands of CTCs from a leukapheresis product requires the ability to deplete 3 to 6 billion WBCs, 50- to 100-fold more cells than devices commonly used for handling 10 mL of whole blood. We addressed this challenge by creating a permeability-enhanced magnetic sorter which utilizes the high magnetic permeability material (iron) in the vicinity of the sorting channels for enhancing magnetic gradients and throughput. This device processes 3 billion WBCs in an hour at a total (sample and buffer) throughput of 168 mL/h, offering ~30-fold-higher cell processing capability per device than existing magnetic sorters (19, 20, 22, 32–36).

To incorporate the high-permeability material, we created two adjoining 1,600-μm-wide channels, one on each side of the sorting channel, and packed these channels with soft magnetic iron particles of ~40 μm in diameter (Fig. 1*B*). This was achieved by dispersing particles in 50% ethanol and then passing them through the empty high-permeability channels where filters at the end of the channels allow fluid to escape while retaining particles, compactly packing the channels (*SI Appendix*, Fig. S4). We used diamond-shaped pillar structures with 25-μm pitch as filters for trapping iron particles. These iron-filled channels can be positioned as close as 25 μm from the sorting channels without risking delamination.

A detailed labeled diagram of the magnetic sorter is shown in Fig. 2. It consists of two stages, which deflect and remove every

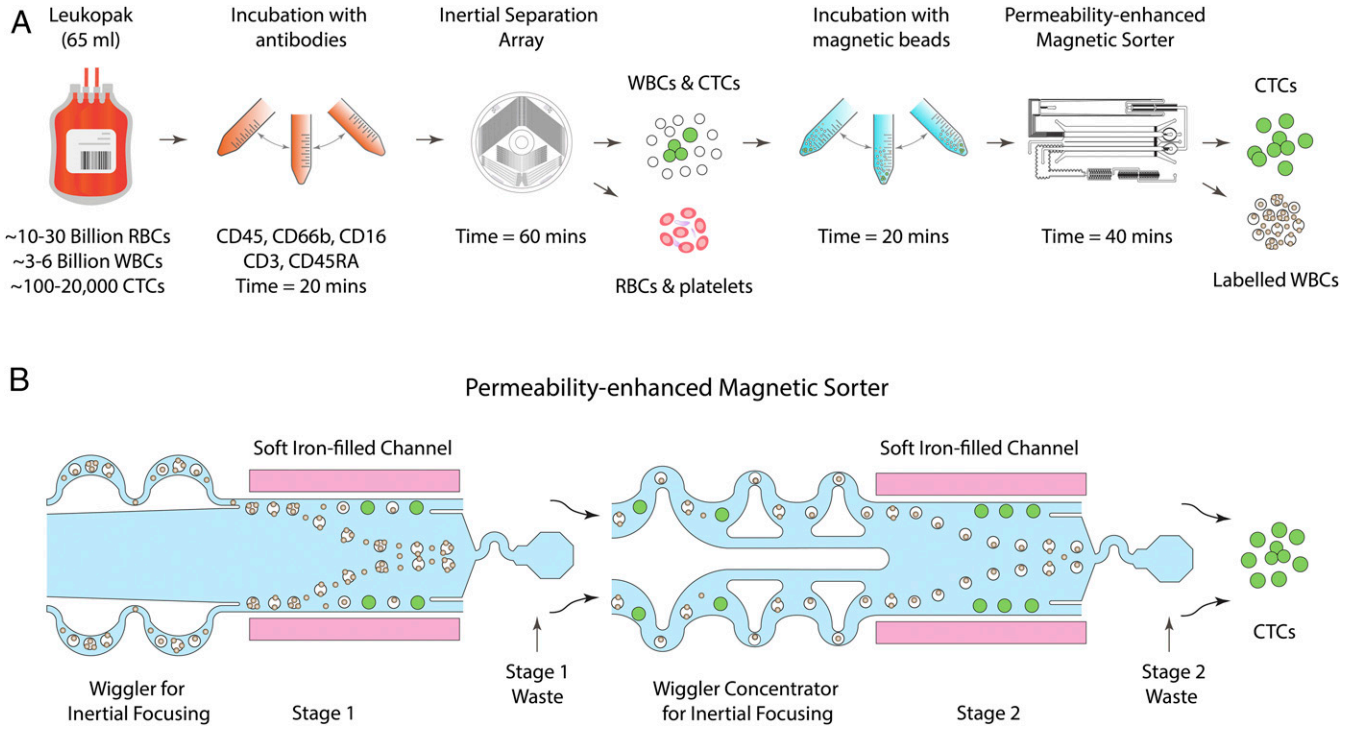

Fig. 1. High-throughput rare CTC separation from full (65 mL) leukapheresis samples. (*A*) Schematics illustrating the microfluidic approach for untouched CTC isolation from leukapheresis products. A leukapheresis product typically contains 3 to 6 billion nucleated cells, from ~5 L of blood volume. We first remove RBCs and platelets from leukapheresis products using size-based inertial separation. It is followed by immunomagnetic removal of WBCs, allowing us to recover untouched CTCs without relying on antigen markers. (*B*) A schematic diagram illustrating the permeability-enhanced magnetic sorter which can deplete ~3 billion WBCs per h from concentrated leukapheresis products. This chip uses two adjoining channels, one on each side of the sorting channels, which are compactly packed with soft magnetic iron particles. These high-permeability channels enhance the magnetic field gradient 35-fold, allowing us to operate at an ultrahigh throughput while deflecting every magnetically labeled cell.

WBC labeled with a 1-μm magnetic bead (Fig. 1*B*). At first, the magnetically labeled cell suspension flows into stage 1 through two sets of microfluidic inlet filters (40-μm aperture) to remove large debris or aggregates (Fig. 2 *A*, 1). Any slender debris smaller in diameter than the aperture of filter 1 are captured based on their length in the tortuous channel geometry of filter 2. After the filters, the cell suspension flows into the stage-1 sorting channel at 48 mL/h via two asymmetric serpentine channels, which inertially focus cells in a single file (Fig. 2 *A*, 2). These serpentine channels utilize a balance between shear-induced lift force and Dean flow-based drag force to focus cells near the center of the serpentine channel (37). At the core of the sorting channel, a buffer flow at 120 mL/h is provided to keep the inertially focused cells close to the channel wall, where magnetic field gradients are at maximum (Fig. 2 *A*, 3). As WBCs move through the deflection channel, they experience a magnetic force and are deflected toward the center of the channel into the stage-1 waste port (Fig. 2 *A*, 4). This provides a clog-free design, where WBCs are deflected into the core of the flow away from the walls and high-gradient regions.

After stage 1, cells flow into stage 2 via another microfluidic filter (40-μm aperture) and two inertial-focusing-based cell concentrators. The cell concentrator works by continuously creating a cell-free region and repeated siphoning using passive flow-controlled resistance (Fig. 2 *A*, 5) (38). In essence, cells pass through asymmetric-inertial focusing units, which create a cell-free region due to inertial lift forces and Dean-flow-induced drag force (*SI Appendix*, Fig. S5). This cell-free region is siphoned away from curved focusing units by a siphoning channel, while cells pass through another focusing unit that creates a new cell-free region, which is siphoned again (*SI Appendix*, Fig. S5). This process is repeated over 140 units until the end of the channel achieving ~20-fold concentration of cells (Fig. 2 *A*, 6). This unit serves two key purposes. First, by concentrating the cells, they are positioned close to the walls in the stage-2 sorting channel where magnetic gradients are maximal; second, after concentration, the excess cell-free fluid is removed through the stage-2 waste port (71%), thus reducing the net flow input into the stage-2 sorting channel (250 μL/min). This provides a greater residence time for cells. Six-feeder channels supply the concentrated cell suspension to the stage-2 sorting channel where any loss in cell focusing is corrected by six inertial focusing units and cells are placed in a single file close to the channel sidewalls (Fig. 2 *A*, 7). In the stage-2 sorting channel, every cell labeled with a bead is deflected to the waste port, while undeflected CTCs (Fig. 2 *A*, 8) are collected within an 11-fold reduced volume. Fig. 2*B* shows an image of the microfabricated polydimethylsiloxane (PDMS) magnetic sorter chip with filled high-permeability channels. The total flow rate (buffer and sample) into the chip is 168 mL/h, demonstrating a remarkable volumetric throughput.

Permeability-Enhanced Magnetophoresis. The ultrahigh-throughput functionality of the magnetic sorter is a direct feature of the unique permeability-enhanced magnetic setup (Fig. 3*A*). We used a quadrupolar arrangement of rectangular (5 × 5 × 40 mm) neodymium–iron–boron (N52 grade) magnets, similar to our previously described first-generation magnetic sorter integrated into the CTC-iChip (19, 20, 22). However, the polarity of magnets is modified to the *y* direction to ensure that the magnetic force on the cells is directed toward the center of the sorting channel in the presence of the adjoining iron-filled channels (Fig. 3 *A* and *B*).

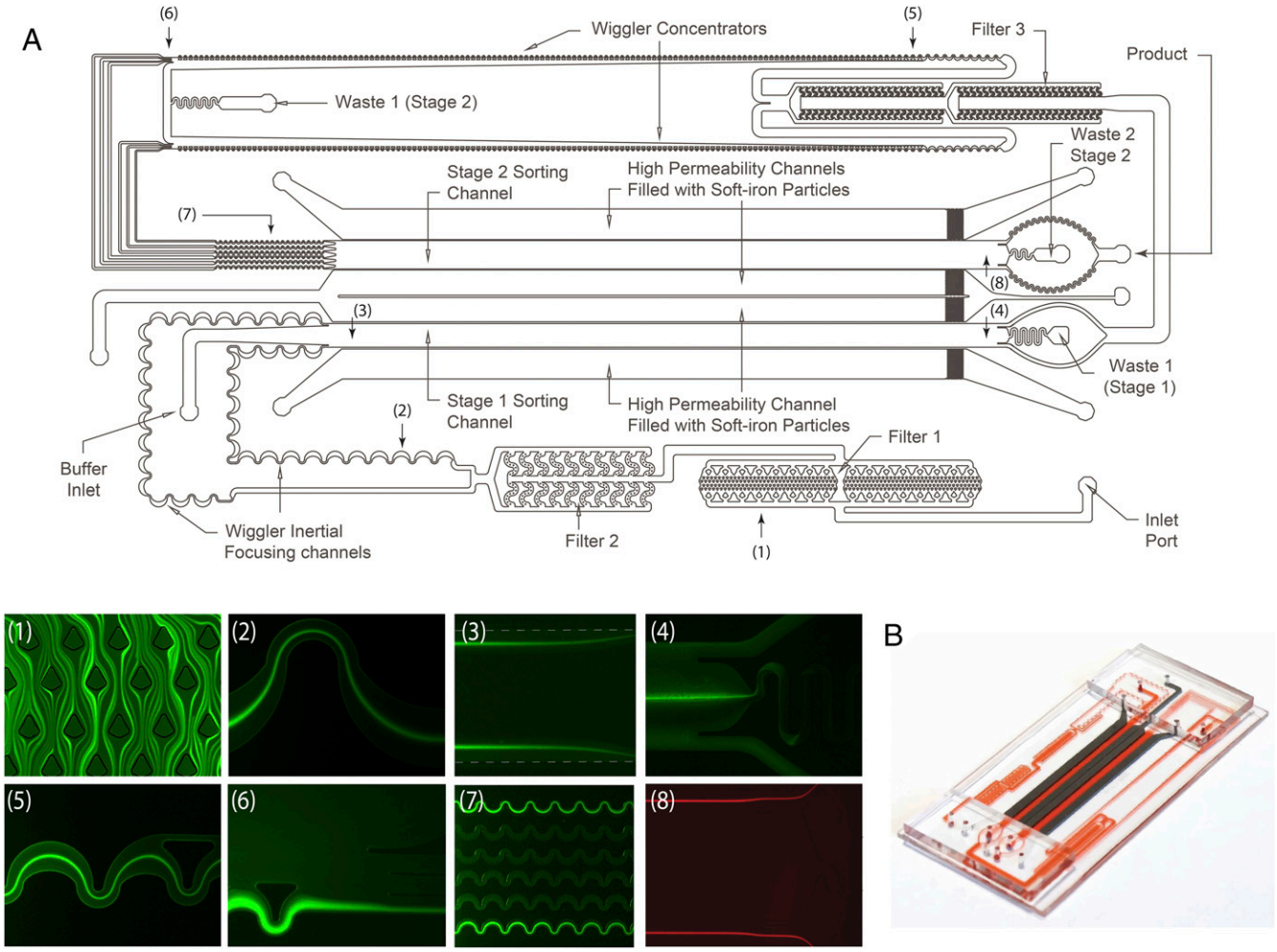

Fig. 2. (*A*) A comprehensive diagram illustrating the microfluidic design of the magnetic sorter. In the first stage, cells flow through microfilters, followed by focusing into single-file streams, which are pinched close to the sidewalls of the sorting channel by buffer flow and WBCs are deflected to the waste port. The rest of the sample flows into stage 2 through a pair of inertial focusing-based microfluidic concentrators. All of the free magnetic beads and every labeled cell are magnetically deflected to the waste port in the stage 2 while the concentrated product is collected. Insets 1 through 7 show fluorescent streak images of WBCs at various positions in the magnetic sorter, from inlet to outlet. Inset 8 shows a fluorescent streak image of isolated CTCs at the product port. (*B*) An image of the microfabricated magnetic sorter device.

Assuming that the superparamagnetic particles used to label cells are saturated, the lateral magnetic force on a labeled cell is directly proportional to the number of particles attached to a cell, and $\partial\left|\vec{B}\right|/\partial y$, the gradient of the norm of the magnetic field $\vec{B}$ in the y direction. To achieve the deflection of a cell labeled with a single bead, increasing the magnetic field gradient is essential for improving the magnetic force and, consequently, the throughput. We therefore incorporated high-permeability channels, filled with soft magnetic iron particles, and also included a 100-μm-thick permalloy strip between the magnets. Under the action of the macro magnetic field from the rectangular magnets, these ferromagnetic microchannels are magnetized and produce a localized magnetic field that decays rapidly, resulting in a high magnetic field gradient in the sorting channel (Fig. 3 *A* and *B*). In addition to the localized field gradient from iron-filled channels, a long-range field gradient from rectangular magnets is also present in the sorting channel but it is significantly (35-fold) smaller. In essence, the high-permeability channels act as on-chip magnetic microlenses and significantly increase the magnetic field gradient. This creates a field gradient as high as 15,400 T/m in deflection channels as compared to the 440 T/m previously achieved by the CTC-iChip magnetic arrangement (20, 22), providing a 35-fold enhancement in magnetic force (Fig. 3*C*).

The increase in magnetic field was experimentally verified by measuring lateral deflection velocity of 2.8-μm superparamagnetic tracer particles with a high-speed camera (Fig. 3*D*). The lateral velocity of the magnetic particles is directly proportional to the field gradient. Given that the magnetic arrangement in the sorter does not allow visualization of the deflection channels, we created a new setup for experimental validation. A 4-mm viewing gap was created between the magnets for direct high-speed imaging of particle trajectories in 800-μm-wide channels with and without adjoining iron channels (*SI Appendix*, Fig. S6). Using particle-tracking velocimetry, we measured up to 54-fold higher lateral velocity with iron channels, demonstrating that the magnetic field gradients are significantly increased in the presence of the high-permeability channels (Fig. 3*D*).

As shown in Fig. 3 *C* and *E*, the magnetic gradient is maximal near the sidewalls of the sorting channels, and it decays progressively toward the center of the channels. Therefore, the microfluidic circuit is designed to inertially arrange and sort cells in a small near-wall region in both the stages. In stage 1, the channel width is 1,500 μm, and the cutoff for deflection is set at

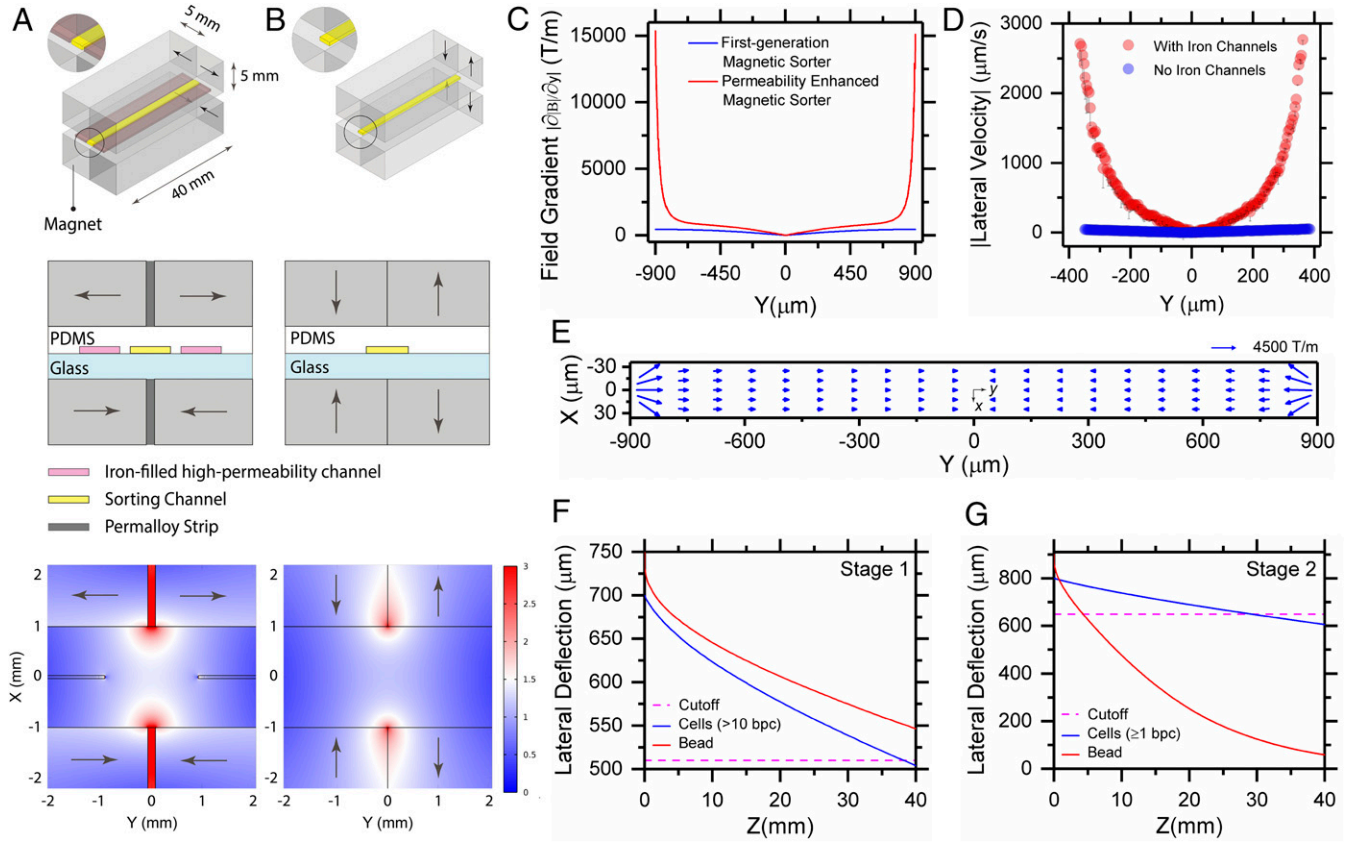

Fig. 3. (*A, Top* and *Middle*) The arrangement of permanent magnets and high-permeability channels in the magnetic sorter. We use N52 grade neodymium-iron-boron (NdFeB) rectangular magnets in a quadrupolar arrangement. (*A*, *Bottom*) The contour plot of the magnetic field intensity. The high-permeability channels and permalloy strips between magnets amplify the magnetic field in the sorting area. (*B*) Arrangement of magnets and corresponding contour plot of the magnetic field in the first-generation magnetic sorter used in the CTC-ichip (22). This sorter does not use high-permeability channels. (*C*) The magnetic field gradient in the permeability-enhanced magnetic sorter and the first-generation magnetic sorter (22). The soft magnetic iron-filled channels act as on-chip magnetic microlenses and increase the magnetic field gradient 35-fold. (*D*) Experimental validation of field enhancement. Using particle-tracking velocimetry, we measured significantly higher lateral deflection velocity of 2.8-μm magnetic beads with iron channels. For directly observing the sorting channel, we used a configuration with a 4-mm gap between magnets as depicted in *SI Appendix*, Fig. S6. (*E*) Vector plot of the gradient of the magnitude of magnetic field in the sorting channel. The vectors are positioned at their respective midpoints. (*F*) Deflection of 1-μm magnetic beads and cells in stage 1. Cells with >10 beads and most of the free beads are deflected to the waste port. (*G*) Lateral deflection of beads and cells in stage 2. All of the free beads and every labeled cell are deflected to the waste port.

240 μm from the sidewalls; in stage 2 the channel width is 1,800 μm, and the cutoff is set at 250 μm from the sidewall (*SI Appendix*, Fig. S7). The height of the channels was kept constant at 60 μm. As evident in the vector plot, a noticeable x component of the gradient is also present in the sidewall region (Fig. 3*E*), but it decays to ∼250 T/m within 100 μm from the sidewall and becomes negligible (<50 T/m) beyond 150 μm from the side wall (*SI Appendix*, Fig. S8*A*). In comparison, the y component of the gradient is more than an order of magnitude stronger in the bulk of the sorting channel. This results in a magnetic force which is predominantly in the lateral y direction in the sorting channel (Fig. 3*E* and *SI Appendix*, Fig. S8*B*). Thus, a cell undergoing magnetophoretic sorting mainly experiences magnetic force toward the center of the channel in the y direction, wall lift force away from the top and bottom walls, and a fluidic viscous drag force (*SI Appendix*, Fig. S8*C*). The wall lift force prevents cells from touching the top and bottom walls as they migrate toward the center of the channel.

Using a laminar velocity profile for a low-aspect-ratio rectangular channel and the magnetic force expression, we calculated the deflection of cells in both the stages. In stage 1, cells having greater than 10 beads along with most of the unbound magnetic beads are deflected to the waste port at a total flow rate of 168 mL/h (Fig. 3*F*). In stage 2, cells are focused 100 μm away from the walls at a flow rate of 250 μL/min. In this stage, free beads and all cells with at least one bead attached to them are deflected (Fig. 3*G*). To execute this high-gradient design, we brought the magnets as close as possible to the chip: The PDMS layer containing the device features was cast as a thin 1-mm layer (same thickness as the bottom glass slide), and magnets were held in a specially designed manifold (*SI Appendix*, Fig. S9).

We also used sequential magnetic labeling to decrease the required number of magnetic beads per cell by ∼91%, thereby lowering the cost burden of the system. This was accomplished by initially labeling WBCs with 10 beads per cell, instead of the previously used concentration of 125 beads per cell (20), thereby depleting >99.5% of WBCs within ∼40 min by using the magnetic sorter (*SI Appendix*, Fig. S10). The remaining 0.5% contaminating WBCs in the product were then relabeled with 125 beads per cell for 10 min and reprocessed through the magnetic sorter in less than 5 min for further removal. We performed the two-step sequential magnetic sorting for all our samples.

Isolation of CTCs. We first tested the performance of the ^{LP}CTC-iChip by recovering ex vivo-cultured CTCs that had been spiked into leukapheresis-mimic samples ($n = 5$), which are produced by

centrifuging approximately a unit of healthy donor blood (400 to 500 mL whole blood) followed by the extraction of the leukocyte-enriched layer. These samples on average contain 1.42 billion WBCs, 56.5 billion RBCs, and 16.9 billion platelets (Fig. 4*A*). The mean volume of the samples was 24.5 mL and the WBC concentration varied from 39.5 to 82.6 million cells per mL at an average concentration of 58.4 million cells per mL, which is ~10-fold higher than the whole blood. The leukapheresis-mimic samples represented approximately a third of the clinical leukapheresis product in volume and the total number of nucleated cells while the concentration of WBCs was similar. In these samples, we spiked 1,000 green fluorescent protein (GFP)-expressing CTCs that had been cultured from viable CTCs enriched from a blood sample of a patient with hormone receptor-positive breast cancer (MGH-BRx-142) (39). Using this approach, we recovered 89.2 ± 5.7% of spiked CTCs and removed 99.96% WBCs (3.35 ± 0.17 $\log_{10}$ depletion), 99.998% RBCs (4.88 ± 0.37 $\log_{10}$ depletion), and 99.998% platelets (4.92 ± 0.15 $\log_{10}$ depletion). We also separately quantified the performance of the inertial separation array module. It removed 99.95% RBCs (3.39 ± 0.28 $\log_{10}$ depletion) and 99.98% platelets (3.83 ± 0.19 $\log_{10}$ depletion). The additional depletion of RBCs and platelets was achieved in stage 2 of the magnetic sorter, since RBCs and platelets are not inertially focused due to their smaller size and removed in the waste channels.

Extending from the mimic samples, we processed three clinical leukapheresis samples containing 5.0 ± 1.0 billion WBCs, 92.6 ± 72.5 billion platelets, and 75.4 ± 66.5 billion RBCs, as shown by red data points in Fig. 4*A*. The WBCs in these samples are representative of a liter of whole blood. The average volume of these full samples was 64.2 ± 4.6 mL (Fig. 4*A*), into which 5,000 MGH-BRx-142 CTCs were spiked. This number of CTCs per leukopak is consistent with previous studies which processed 5% of clinical leukapheresis samples, calculating that, if technically feasible, screening of the entire leukopak would have produced >10,000 CTCs (24).

Depending on the apheresis operating conditions, the WBC concentration in these leukapheresis samples varied from 61 to 90 million cells per mL, while platelet concentrations ranged between 70 and 3,043 million platelets per mL. Even though platelet and WBC concentrations were more than 10-fold higher than whole blood, two parallel ^{LP}CTC-iChips effectively removed 99.97% WBCs (3.55 ± 0.26 $\log_{10}$ purification) while recovering 4,305 CTCs out of the 5,000 spiked CTCs (86.1 ± 0.6% yield) at an average purity of 0.3% (Fig. 4*B*). The device also depleted >99.999% RBCs (5.11 ± 0.35 $\log_{10}$ purification) and >99.999% platelets (5.08 ± 0.41 $\log_{10}$ purification), demonstrating a highly efficient microfluidic removal of contaminating RBCs and platelets (Fig. 4*A*). The isolation process preserved the CTC morphology as

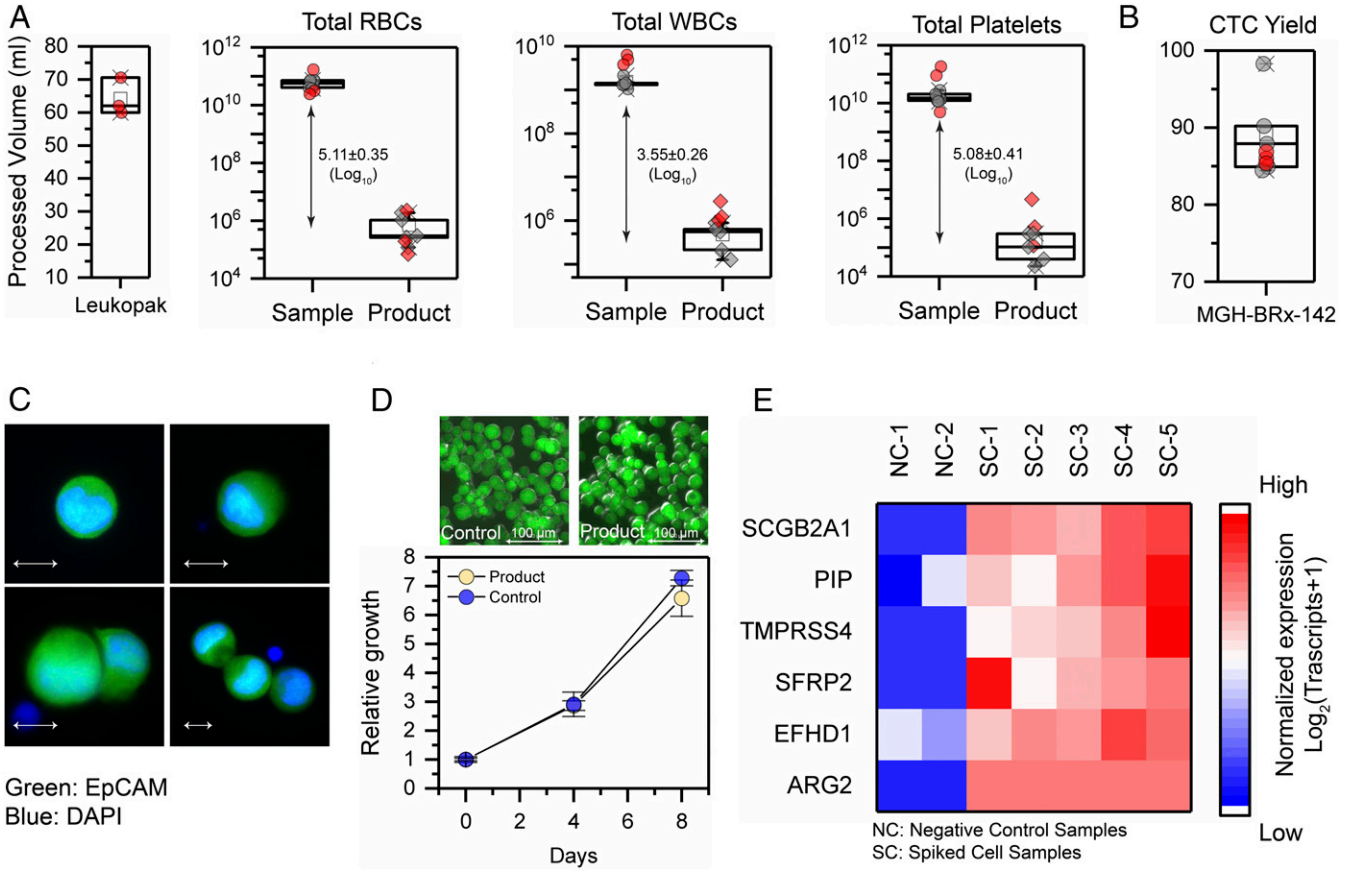

Fig. 4. (*A*) Processed leukopak sample volumes, depletion data and cell numbers in full leukapheresis samples (shown by red symbols, $n = 3$), mimic samples (shown by gray symbols, $n = 5$), and in the isolated product. On average, we processed 64.2 ± 4.6 mL leukapheresis samples. We achieved 5.11, 3.55, and 5.08 $\log_{10}$ depletion of RBCs, WBCs, and platelets, respectively. (*B*) CTC isolation yield. In leukapheresis samples, we recovered 86.1% spiked MGH-BRx-142 cells ($n = 3$), while mimic samples had a slightly higher yield of 89.2% cells ($n = 5$). (*C*) Immunofluorescence images of isolated spiked MGH-BRx-142 CTCs stained with EpCAM (green) and DAPI (blue). (Scale bar, 10 μm.) (*D*) Relative in vitro growth of isolated CTCs in product vs. control as measured by the amount of ATP present in the cells ($n = 3$). The inset panels show images of the cultured MGH-BRx-142 cells. (Scale bar, 100 μm.) (*E*) Expression of the breast lineage markers from spiked MGH-BRx-142 cells after CTC enrichment as measured by ddPCR analysis. Negative controls are healthy donor samples in which no CTCs were spiked.

demonstrated by a gallery of EpCAM- and DAPI-stained CTCs in Fig. 4*C*.

Postisolation, we tested a fraction of the product (40%) for in vitro culture to assess whether the microfluidic devices damage the proliferative properties of isolated CTCs. Enriched CTCs from the product proliferated comparably with control samples (Fig. 4*D*). We have recently described an RNA-based droplet digital PCR (ddPCR) assay for absolute quantitation of tissue-lineage-specific transcripts from CTCs in the background of normal blood cells (8, 9). The ddPCR assay confirmed the isolation of cells with intact RNA, suitable for molecular analyses (Fig. 4*E*). To mimic clinical situations in which CTC numbers are extremely low, such as early cancer detection applications, we tested the magnetic sorter by spiking only five GFP-labeled cells from different cell lines including the breast CTC line MGH-BRx-142, the commonly studied breast cancer line MDA-MB-231, and the prostate cancer line LNCaP, using the leukopak mimic assay (*SI Appendix*, Fig. S11). For precise quantitation of the number of cancer cells spiked into the leukopak mimics, cells were individually picked using single-cell micromanipulation and we conducted five independent CTC spiking experiments for each cell line. Using MGH-BRx-142, we recovered four of five spiked cells in two experiments and five of five in another three experiments. Similarly, for MDA-MB-231, we detected four of five cells in three spiking experiments and five of five cells in two other experiments. Using prostate LNCaP cells, we successfully recovered five of five spiked cells in all of the five experiments.

Discussion

We have described an ultrahigh-throughput semiautomated microfluidic technology, making use of approaches to high-capacity magnetic cell depletion, to sort through an entire leukapheresis product for the presence of CTCs within 3 h. Compared to current technologies, this strategy increases the number of cancer cells recovered by two orders of magnitude, and it may, therefore, provide a noninvasive alternative to core needle biopsies of tumors that are routinely used for cancer diagnosis and monitoring. Existing CTC isolation technologies are inherently limited by the minute number of CTCs present within a standard 10-mL tube of whole blood. While these have provided important insights into the process of blood-borne metastasis (40–42), the incorporation of CTC-based diagnostics into clinical care requires consistent isolation of sufficient numbers of cancer cells from the blood. The only feasible avenue to capture more CTCs is to increase the volume of processed blood. Poisson-distribution-based statistical modeling of random CTC sampling in blood indicates that the probability of obtaining CTCs increases predictably with the processed blood volume and CTC concentration (*SI Appendix*, Fig. S1) (43), and a leukapheresis product, generated from ∼5 L of blood, is the ideal starting material. However, microfluidic enrichment of cancer cells from such a large number of blood cells presents multiple technological challenges, particularly using antibody-mediated negative depletion of massive numbers of WBCs to reveal untagged viable CTCs. To this end, the ^{LP}CTC-iChip efficiently processes a large concentrate of blood cells, namely 65 mL of leukapheresis product with more than 10-fold higher concentration of WBCs and platelets compared with the peripheral blood. Operating at an ultrahigh throughput, the ^{LP}CTC-iChip achieves 86% CTC recovery with greater than 10^5 depletion of hematopoietic cells, without clogging, platelet activation, or release of WBC DNA nets. Recovered CTCs have preserved viability and molecular integrity. Unlike macro cell-sorting approaches such as density gradient centrifugation and bulk magnetic sorting (31), the ^{LP}CTC-iChip is operator-independent, incurs minimal rare cell loss, and provides precise sorting conditions at a single-cell level.

Negative depletion of hematopoietic cells, as opposed to the positive selection of CTCs, presents important biological advantages. As noted in earlier studies, EpCAM-based positive selection of CTCs from a large background of untagged blood cells requires less magnetic sorting (24, 27, 28), but it also limits the types of cancer cells recovered to the subset expressing high levels of this epithelial marker. In addition, the presence of bead-conjugated capturing antibodies at the tumor cell surface restricts their functional viability, the quality of their RNA, and their accessibility for detailed imaging and morphological analysis. In contrast, negative depletion of hematopoietic cells generates unmanipulated and potentially viable CTCs.

The key innovation in the ^{LP}CTC-iChip is the powerful magnetic sorter, which uses high magnetic gradients generated by iron-filled channels, acting as magnetic microlenses to achieve significantly higher (30-fold) cell deflection than traditional magnetic sorters (19, 20, 22, 32–36). To our knowledge, the microfluidic introduction of high-permeability material by compactly packing channels with iron particles has not been previously demonstrated. It presents a simple room-temperature-compatible manufacturing technique for creating high-gradient magnetic fields while allowing full lithographic control over the shape and positioning of the iron-filled channels. In contrast to conventional techniques that require complex microfabrication and high-temperature processes, such as metal deposition, etching, electroplating, and planarization (34, 35, 44), our approach can be readily integrated with the plastic microfluidic devices, making it highly conducive to scale-up and fabrication.

The magnetic sorting technology differs from previously reported devices including a free-flow magnetophoresis platform described by Pamme and Wilhelm (32) and Robert et al. (45), sorting up to 0.5 million cells per hour, and a multiplexed magnetic sorter developed by Adams et al. (34), in which different strains of *Escherichia coli* are sorted with different-sized magnetic beads (2.8 and 4.5 μm diameter). Kelley and coworkers (35) demonstrated a positive selection-based CTC sorter chip, albeit with a limited throughput of ∼10,000 cells per h, subsequently enhanced to achieve flows of 30 million cells per h for use in CRISPR-Cas9 phenotype screening assays (36). As a component of the CTC-iChip platform, our group has previously developed a magnetic cell sorter based on a quadripolar magnetic arrangement, which can sort WBCs at a throughput of 50 million cells per h and efficiently recover CTCs (19, 20, 22). However, all of these platforms have limited cell-processing capability and cannot handle the 10-fold increased concentration of WBCs and large volume of leukapheresis products.

In developing the permeability-enhanced magnetic sorter, we addressed two major technical challenges. First, we developed a magnetic circuit sensitive enough to deflect all of the unbound beads, thus removing any possibility of bead contamination in the product. Second, despite using high field gradients, we created a clog-free microfluidic design. During labeling, some of the WBCs disproportionately acquire a large number of beads (>50 beads), due to their high expression of the antigens targeted for depletion. Under the action of traditional magnetic field design, cells with high bead loads will rapidly attach to the channel walls, forming a plaque that clogs the channel, leading to device failure. Indeed, most previously reported high-gradient magnetic sorters position ferromagnetic tracks below the bottom wall of the channel, causing tagged cells to deflect either toward the top or the bottom walls of the channel, creating a high likelihood of WBCs clogging at high-throughput operation (34, 35, 44). We prevented this complication in our magnetic sorter design by deflecting cells toward the center of the channel in the core of the flow where no walls are present, and away from high-gradient regions; cells with high magnetic loads are rapidly focused at the center of the channel, thus creating an inherently safe design which can process billions of cells. The symmetric force toward the center of the channel is made possible by coplanar high-permeability channels. To further increase throughput, the magnetic sorter may be parallelized by including six devices within a single monolithic plastic disk, which would push the

cell-processing throughput to unprecedented levels of 18 billion cells per h.

Recently, various in vivo approaches have been proposed to increase the volume of processed blood, and hence the number of recovered CTCs. Nagrath and coworkers (46) proposed an intravascular aphaeretic system, whereby blood is processed through anti-EpCAM-coated herringbone channels for a positive selection of CTCs. Other investigators have also proposed an indwelling functionalized medical wire, named CellCollector, for continuous collection of CTCs from the blood (47) and an intravascular magnetic wire for in vivo immunomagnetic capture of CTCs, following in vivo labeling of cells with magnetic particles (48). While tested in animal models, the invasiveness of these approaches may preclude clinical applications, and the number and viability of CTCs recovered through in vivo implanted devices remains to be determined. In contrast, leukapheresis is a routinely performed standard clinical procedure which is well tolerated by cancer patients undergoing active therapy and is compatible with planned medical and surgical interventions (23–28). Recent reports have demonstrated that the application of standard CTC enrichment technologies to such pre-enriched WBCs, including the CellSearch EpCAM-based positive selection method (24), greatly increases CTC recovery (23–28). However, the very high concentration of mononuclear cells in leukopaks precludes analysis of the entire leukapheresis product using standard CTC recovery techniques, and recent studies have analyzed only 5% of leukopaks (200 million cells), representing only a fivefold increase over the standard 10-mL tube of whole blood (20, 22). Even with this caveat, Lambros et al. (24) recovered a median 1,918 CTCs from 14 patients with metastatic prostate cancer, predicting that, if possible, analysis of the entire leukopak would have generated an average recovery of 12,546 CTCs. These findings support the use of leukapheresis as a viable strategy for robust CTC detection and analysis but also point to the critical need for technologies, such as presented here, capable of sorting through the entire leukapheresis product, with 100-fold increased yield over the currently used 10 mL of whole blood.

One of the limitations of the current approach is the multistep nature of the protocol. The removal of RBCs, platelets, and WBCs is performed using two separate fluidically unconnected devices, creating opportunities for CTC loss during transfer between the two chips. In future, we plan to address this limitation by serially integrating inertial separation array devices and magnetic sorter in the form of a single monolithic plastic chip, which would reduce the transfer steps, minimize the isolation time to less than 2 h, and simplify the assay. The second limitation is that the current approach loses very rare CTCs that may travel in association with WBCs (49). To prevent this loss, we are planning to incorporate a recently developed size-based CTC cluster chip (50) as the first step in our protocol to isolate CTC clusters and CTC–WBC clusters in a clean buffer.

Major advances in plasma circulating tumor DNA analyses are poised to revolutionize the field of clinical oncology, enabling on-treatment monitoring for acquired drug-resistance mutations, monitoring tumor burden, and ultimately earlier detection of cancer (42). With robust technologies such as presented here, CTC analyses performed on leukapheresis products will extend the reach of liquid biopsies in metastatic cancer, enabling a broad range of additional molecular analyses, including RNA and protein-based determinations and whole-cell analyses, which currently require direct biopsies of metastatic lesions. These include quantitation of cell-surface proteins on cancer cells to guide immune checkpoint therapies or antibody–drug conjugates; pharmacokinetic measurements to assess the effect of therapeutic interventions on their targeted intracellular signaling pathways, and defining molecular mechanisms of acquired cancer drug resistance (8, 21); and real-time generation of tumor-cell-derived cultures for individualized functional drug sensitivity testing (5). Single-cell-resolution analyses also enable critical studies of cancer heterogeneity, including the detection of early resistant colonies that foretell the emergence of clinical drug resistance (39) and molecular analyses of heterogeneity among metastatic precursors that underlie the blood-borne spread of cancer. Importantly, since CTCs may be shed by invasive cancers long before metastases are established, leukapheresis combined with CTC detection may play a critical role in screening high-risk patients for early cancer, identifying the tissue of origin and reducing the need for invasive biopsies. In this context, CTC-based analyses may be combined with plasma-based screening for mutations or aberrant DNA methylation patterns, providing a comprehensive approach to noninvasive early cancer detection. While the focus of our ^{LP}CTC-iChip analysis has been on rare cancer cell isolation from large blood volumes, reversing the magnetic antibody selection from negative depletion of blood cells to positive selection of rare cells in the blood may also be applicable in diverse areas such as stem cell isolation (51), enrichment of rare immune cell subsets including antibody-producing cells and cancer-reactive lymphocytes (52), phenotypic screening assays (36), and pathogen detection (34). Thus, microfluidic technology for ultrahigh-throughput magnetic sorting of rare cells within very large blood volumes will provide exceptional opportunities to characterize the full complexity of blood and establish novel clinical applications.

Materials and Methods

Experimental protocols reviewed and authorized by the Massachusetts General Hospital (MGH) Institutional Review Board were used to obtain informed consent for whole-blood donations from internal healthy donors (Protocol 2009-P-000295) and the MGH blood bank (Protocol 2015-P-000656), respectively. In some cases, healthy donor whole-blood samples were also procured from Research Blood Components, LLC. Healthy donor leukapheresis and leukapheresis-mimic samples were purchased from anonymous donors at MGH blood bank under an Institutional Review Board–exempt protocol. Some of the leukapheresis products were commercially purchased from Key Biologics LLC. The magnetic sorter was fabricated using a PDMS soft lithography technique and the inertial separation array devices were fabricated with medical-grade cyclic olefin copolymer. For labeling WBCs, 1-μm MyOne Streptavidin T1 beads (Invitrogen) were used. Detailed experimental procedures can be found in *SI Appendix*.

Data Availability. All data discussed are included within the paper and *SI Appendix*.

ACKNOWLEDGMENTS. We appreciate the blood donors whose contributions have enabled this work. This work was supported by the National Institute of Biomedical Imaging and Bioengineering (P41EB002503 and U01 EB012493), by the National Cancer Institute (U01CA214297, 2RO1CA129933, and R01CA226871), by the American Cancer Society (132030-RSG-18-108-01-TBG), and by the Howard Hughes Medical Institute. N.M.K. was supported by Shriners Hospital for Children (Mass Spectrometry Special Shared Facility) and Harvard Medical School Eleanor and Miles Shore Faculty Fellowship Award. The authors thank Dr. Marcela Maus for help in obtaining leukopaks; Mark Kalinich, Kaustav Gopinathan, and Onur Tasci for useful discussions; and Octavio Hurtado along with Maedeh Roushan for microfabrication assistance.

1. N. Riggi, M. Aguet, I. Stamenkovic, Cancer metastasis: A reappraisal of its underlying mechanisms and their relevance to treatment. *Annu. Rev. Pathol.* **13**, 117–140 (2018).
2. W. J. Allard *et al.*, Tumor cells circulate in the peripheral blood of all major carcinomas but not in healthy subjects or patients with nonmalignant diseases. *Clin. Cancer Res.* **10**, 6897–6904 (2004).
3. N. Aceto *et al.*, Circulating tumor cell clusters are oligoclonal precursors of breast cancer metastasis. *Cell* **158**, 1110–1122 (2014).
4. P. S. Steeg, Targeting metastasis. *Nat. Rev. Cancer* **16**, 201–218 (2016).
5. M. Yu *et al.*, Cancer therapy. Ex vivo culture of circulating breast tumor cells for individualized testing of drug susceptibility. *Science* **345**, 216–220 (2014).

6. D. T. Miyamoto *et al*., An RNA-based digital circulating tumor cell signature is predictive of drug response and early dissemination in prostate cancer. *Cancer Discov.* **8**, 288–303 (2018).
7. X. Hong *et al*., Molecular signatures of circulating melanoma cells for monitoring early response to immune checkpoint therapy. *Proc. Natl. Acad. Sci. U.S.A.* **115**, 2467–2472 (2018).
8. T. T. Kwan *et al*., A digital rna signature of circulating tumor cells predicting early therapeutic response in localized and metastatic breast cancer. *Cancer Discov.* **8**, 1286–1299 (2018).
9. M. Kalinich *et al*., An RNA-based signature enables high specificity detection of circulating tumor cells in hepatocellular carcinoma. *Proc. Natl. Acad. Sci. U.S.A.* **114**, 1123–1128 (2017).
10. S. Manier *et al*., Whole-exome sequencing of cell-free DNA and circulating tumor cells in multiple myeloma. *Nat. Commun.* **9**, 1691 (2018).
11. E. A. Punnoose *et al*., Evaluation of circulating tumor cells and circulating tumor DNA in non-small cell lung cancer: Association with clinical endpoints in a phase II clinical trial of pertuzumab and erlotinib. *Clin. Cancer Res.* **18**, 2391–2401 (2012).
12. S. Nagrath *et al*., Isolation of rare circulating tumour cells in cancer patients by microchip technology. *Nature* **450**, 1235–1239 (2007).
13. M. Ebrahim *et al*., Ultra-fast, label-free isolation of circulating tumor cells from blood using spiral microfluidics. *Nat. Protoc.* **11**, 134–148 (2016).
14. A. F. Sarioglu *et al*., A microfluidic device for label-free, physical capture of circulating tumor cell clusters. *Nat. Methods* **12**, 685–691 (2015).
15. C. Renier *et al*., Label-free isolation of prostate circulating tumor cells using Vortex microfluidic technology. *npj Precis. Oncol.* **1**, 15 (2017).
16. J. Shaw Bagnall *et al*., Deformability of tumor cells versus blood cells. *Sci. Rep.* **5**, 18542 (2015).
17. E. S. Park *et al*., Continuous flow deformability-based separation of circulating tumor cells using microfluidic ratchets. *Small* **12**, 1909–1919 (2016).
18. S. L. Stott *et al*., Isolation of circulating tumor cells using a microvortex-generating herringbone-chip. *Proc. Natl. Acad. Sci. U.S.A.* **107**, 18392–18397 (2010).
19. E. Ozkumur *et al*., Inertial focusing for tumor antigen-dependent and -independent sorting of rare circulating tumor cells. *Sci. Transl. Med.* **5**, 179ra47 (2013).
20. N. M. Karabacak *et al*., Microfluidic, marker-free isolation of circulating tumor cells from blood samples. *Nat. Protoc.* **9**, 694–710 (2014).
21. D. T. Miyamoto *et al*., RNA-Seq of single prostate CTCs implicates noncanonical Wnt signaling in antiandrogen resistance. *Science* **349**, 1351–1356 (2015).
22. F. Fachin *et al*., Monolithic chip for high-throughput blood cell depletion to sort rare circulating tumor cells. *Sci. Rep.* **7**, 10936 (2017).
23. T. N. Fehm *et al*., Diagnostic leukapheresis for CTC analysis in breast cancer patients: CTC frequency, clinical experiences and recommendations for standardized reporting. *Cytometry A* **93**, 1213–1219 (2018).
24. M. B. Lambros *et al*., Single-cell analyses of prostate cancer liquid biopsies acquired by apheresis. *Clin. Cancer Res.* **24**, 5635–5644 (2018).
25. A. Franken *et al*., Label-free enrichment and molecular characterization of viable circulating tumor cells from diagnostic leukapheresis products. *Clin. Chem.* **65**, 549–558 (2019).
26. F. Reinhardt *et al*., Diagnostic leukapheresis enables reliable transcriptomic profiling of single circulating tumor cells to characterize inter-cellular heterogeneity in terms of endocrine resistance. *Cancers (Basel)* **11**, 903 (2019).
27. J. C. Fischer *et al*., Diagnostic leukapheresis enables reliable detection of circulating tumor cells of nonmetastatic cancer patients. *Proc. Natl. Acad. Sci. U.S.A.* **110**, 16580–16585 (2013).
28. K. C. Andree *et al*., Toward a real liquid biopsy in metastatic breast and prostate cancer: Diagnostic LeukApheresis increases CTC yields in a European prospective multicenter study (CTCTrap). *Int. J. Cancer* **143**, 2584–2591 (2018).
29. B. R. Mutlu *et al*., Non-equilibrium inertial separation array for high-throughput, large-volume blood fractionation. *Sci. Rep.* **7**, 9915 (2017).
30. L. R. Huang, E. C. Cox, R. H. Austin, J. C. Sturm, Continuous particle separation through deterministic lateral displacement. *Science* **304**, 987–990 (2004).
31. O. Lara, X. Tong, M. Zborowski, J. J. Chalmers, Enrichment of rare cancer cells through depletion of normal cells using density and flow-through, immunomagnetic cell separation. *Exp. Hematol.* **32**, 891–904 (2004).
32. N. Pamme, C. Wilhelm, Continuous sorting of magnetic cells via on-chip free-flow magnetophoresis. *Lab Chip* **6**, 974–980 (2006).
33. N. Pamme, Magnetism and microfluidics. *Lab Chip* **6**, 24–38 (2006).
34. J. D. Adams, U. Kim, H. T. Soh, Multitarget magnetic activated cell sorter. *Proc. Natl. Acad. Sci. U.S.A.* **105**, 18165–18170 (2008).
35. P. M. Aldridge *et al*., Prismatic deflection of live tumor cells and cell clusters. *ACS Nano* **12**, 12692–12700 (2018).
36. B. Mair *et al*., High-throughput genome-wide phenotypic screening via immunomagnetic cell sorting. *Nat. Biomed. Eng.* **3**, 796–805 (2019).
37. D. Di Carlo, D. Irimia, R. G. Tompkins, M. Toner, Continuous inertial focusing, ordering, and separation of particles in microchannels. *Proc. Natl. Acad. Sci. U.S.A.* **104**, 18892–18897 (2007).
38. J. M. Martel *et al*., Continuous flow microfluidic bioparticle concentrator. *Sci. Rep.* **5**, 11300 (2015).
39. N. V. Jordan *et al*., HER2 expression identifies dynamic functional states within circulating breast cancer cells. *Nature* **537**, 102–106 (2016).
40. D. S. Micalizzi, S. Maheswaran, D. A. Haber, A conduit to metastasis: Circulating tumor cell biology. *Genes Dev.* **31**, 1827–1840 (2017).
41. M. Yu *et al*., Circulating breast tumor cells exhibit dynamic changes in epithelial and mesenchymal composition. *Science* **339**, 580–584 (2013).
42. D. A. Haber, V. E. Velculescu, Blood-based analyses of cancer: Circulating tumor cells and circulating tumor DNA. *Cancer Discov.* **4**, 650–661 (2014).
43. A. G. J. Tibbe, M. C. Miller, L. W. M. M. Terstappen, Statistical considerations for enumeration of circulating tumor cells. *Cytometry A* **71**, 154–162 (2007).
44. D. W. Inglis, R. Riehn, J. C. Sturm, R. H. Austin, Microfluidic high gradient magnetic cell separation. *J. Appl. Phys.* **99**, 08K101 (2006).
45. D. Robert *et al*., Cell sorting by endocytotic capacity in a microfluidic magnetophoresis device. *Lab Chip* **11**, 1902–1910 (2011).
46. T. H. Kim *et al*., A temporary indwelling intravascular aphaeretic system for in vivo enrichment of circulating tumor cells. *Nat. Commun.* **10**, 1478 (2019).
47. N. Saucedo-Zeni *et al*., A novel method for the in vivo isolation of circulating tumor cells from peripheral blood of cancer patients using a functionalized and structured medical wire. *Int. J. Oncol.* **41**, 1241–1250 (2012).
48. O. Vermesh *et al*., An intravascular magnetic wire for the high-throughput retrieval of circulating tumour cells in vivo. *Nat. Biomed. Eng.* **2**, 696–705 (2018).
49. B. M. Szczerba *et al*., Neutrophils escort circulating tumour cells to enable cell cycle progression. *Nature* **566**, 553–557 (2019).
50. J. F. Edd *et al*., Microfluidic concentration and separation of circulating tumor cell clusters from large blood volumes. *Lab Chip* **20**, 558–567 (2020).
51. B. Zhu, S. K. Murthy, Stem cell separation technologies. *Curr. Opin. Chem. Eng.* **2**, 3–7 (2013).
52. C. A. Klebanoff, L. Gattinoni, N. P. Restifo, Sorting through subsets: Which T-cell populations mediate highly effective adoptive immunotherapy? *J. Immunother.* **35**, 651–660 (2012).